

Carcinoembryonic Antigen Immunosensor Developed with Organoclay Nanogold Composite Film

Justin Claude Kemmegne-Mbouguen^{1,2,*}, Emmanuel Ngameni¹, Priscilla G. Baker², Tesfaye T. Waryo^{2,*}, Boitumelo Kgarebe² and Emmanuel I. Iwuoha²

¹ Laboratoire de Chimie Analytique, Faculté des sciences, Université de Yaoundé I, B.P. 812 Yaoundé, Cameroun

² SensorLab, Department of Chemistry, University of Western Cape, Bellville, Cape Town, 7535, South Africa.

*E-mail: jkemmeg@yahoo.fr; twaryo@uwc.ac.za

Received: 11 September 2013 / Accepted: 4 November 2013 / Published: 15 November 2013

Organoclay nanogold composite were prepared using gold nanoparticles and the natural Cameroonian clay grafted with amino organosilane. The fonctionnalization of clay provided abundant amino group to assemble gold nanoparticles. A label-free electrochemical immunosensor for the sensitive determination of carcinoembryonic antigen (CEA) was fabricated by immobilizing anti-CEA onto organoclay nanogold composite film modified electrode by the cross-linking method using glutaraldehyde. In addition, the preparation procedure of the immunosensor was investigated by cyclic voltammetry (CV) and electrochemical impedance spectroscopy (EIS). Under optimal conditions, the resulting immunosensor displayed a high sensitivity for the detection of CEA, and responded to the CEA concentration in two ranges from 0.05 to 5.0 ng/mL ($R = 0.991$) and from 5.0 to 120.0 ng/mL ($R = 0.998$) with a detection limit of 0.01 ng/mL.

Keywords: Organoclay, nanogold composite, modified electrode, immunosensor, and carcinoembryonic antigen

1. INTRODUCTION

Since their introduction in electrochemistry field in 1983 by Gosh and Bard[1], clay modified electrodes have been and are still a very attractive research area. Clay minerals were found to be interesting for the elaboration of electrochemical sensor and biosensors, because of their great specific area, swelling and porosity properties, good catalytic support as well as low cost, thermal and mechanical stabilities [2; 3; 4].Despite these attractive properties, pristine clay minerals suffer from

poor selectivity and restricted adsorption capacities. These limitations can be overcome by their functionalization with specific organic groups, leading to hybrid materials with new pattern of reactivity, selectivity or sensitivity when they are used to form thin films onto an electrode surface. Several methods reported in literature including: intercalation of organic molecules in the interlayer space [5; 6], post-synthesis grafting of organosilane onto clay surfaces [7; 8] and the one-step preparation of organoclay by the sol gel process [9; 10] are used to functionalize clay. Despite their insulating character, clay and organoclay modified electrodes in the presence of redox mediator were successfully exploited for applications in the field of electrochemical sensors and PPO biosensors [11; 12; 13].

In recent years, research on nanomaterials has increased tremendously because of their importance as potential building blocks for a variety of nanoscale biomedical, bioanalytical, bioseparation and bioimaging applications [14; 15; 16]. The utilities of nanoparticles (NP) strongly depend upon their physicochemical characteristics and their interaction with various surface moieties. Gold nanoparticles stand apart from other nanoparticles and quantum dots because of their biocompatibility [17]. Thus they have been extensively used as matrices for the immobilization of macromolecules such as proteins, enzymes and antibodies; as well as chemical labels for biomolecules [17]. The presence of gold nanoparticles (AuNP) provides more freedom in the orientation for the anchored protein molecules and hence maximizes the utilization of their bioactive sites, thus permitting proteins to orient for direct electron transfer. Because of their large surface areas and good electronic properties [18; 19; 20; 21], gold nanoparticles provide a stable surface for enzyme immobilization and allow the electrochemical sensing to be performed without the need of external electron-transfer mediators. They have been used as intermediators to immobilize antibody to efficiently retain their activity and to enhance current response in the construction of a sensitive amperometric immunosensor [16; 22; 23; 24; 25; 26]. For example, Wang et al reported the use of nanogold as intermedicator to immobilize of CEA antibody on chitosan modified GCEs for sensitive detection of CEA [27]. Cao et al immobilize casein antibody on poly(L-Arginine)/multi-walled carbon nanotube composite film via nanogold particles for casein detection [25]. Along the same line, Ga et al used nanogold nanoparticles to immobilize HIV p24 antibody on poly(L-lysine) and mercapto succinic acid modified gold electrode for HIV detection [28]. Till now, however, the use of organically functionalized clay bearing organic groups covalently attached to clay particles remains unexplored in affinity biosensor [4].

It is well known that some functional groups such as cyano ($-\text{CN}$), mercapto ($-\text{SH}$), and amino ($-\text{NH}_2$) groups have a high affinity for Au. Therefore, nano-Au/organoclay composite was prepared via covalent bonds between gold nanoparticles and the $-\text{NH}_2$ groups of the functionalized amino clay. This material has combined the advantages of inorganic nanoparticles and clay, providing a suitable microenvironment to immobilize protein. In the present work, we report the synthesis nanogold organoclay composite, their use to modify glassy carbon electrode and to immobilize CEA via a crosslink agent, and polyphenol oxidase on the electrode and their possible application as affinity and mediatorless catalytic biosensors for sensitive and selective detection of CEA and phenol respectively. These substrates were chosen because of their importance in health and environment. Carcinoembryonic antigen (CEA) is an important tumor marker responsible for clinical diagnosis of

over 95% of all colon tumors, 50% of breast tumors, as well as tumors of the lung cancer, ovarian carcinoma, cystadeno carcinoma [29; 30; 31; 32; 33].

2. EXPERIMENTAL

2.1. Material, Chemicals and Reagents

The clay sample used in this study, named “Ba”, was collected in a deposit on Baba hill in West Cameroon (Central Africa). It is formed mainly of smectite with minor amounts of feldspar. Its full chemical analysis and physicochemical characteristics are provided elsewhere [29]. Baba clay is characterised by a surface area (N_2 , B.E.T) of $86 \text{ m}^2 \text{ g}^{-1}$ and a cation exchange capacity (C.E.C) of 8 meq g^{-1} . The grafting agent used here was γ -aminopropyltrimethoxysilane (APTES). This grafting agent and toluene were purchased from Sigma Aldrich. The organoclay was prepared using homoionic fine fraction (particle size below $2 \mu\text{m}$). This fraction was separated by sedimentation of pristine clay converted in its sodium form and collected by a procedure previously described [34].

Carcinoembryonic antigen (CEA) and anti-CEA were purchased from Bocon. Bovine serum albumin (BSA, 99%), glutaraldehyde, gold chloride (HAuCl_4), sodium borohydride (NaBH_4) were bought from Sigma. All other chemicals and reagents used in the electrochemical studies were of analytical grade and used as received. Ascorbic acid, K_2HPO_4 (99%), KH_2PO_4 (99%), $\text{K}_4\text{Fe}(\text{CN})_6$ (99%), $\text{K}_3\text{Fe}(\text{CN})_6$ (> 99%), NaCl (99.5%) and KCl (99.5%), NaOH and 37 % HCl were purchased from Sigma. The CEA was stored in the frozen state, and its standard solutions were prepared freshly with bi-distilled water when in used.

2.2. Preparation of organoclaynanogold composite.

a) Preparation of organoclay

The first step was the treatment of homoionic clay with an organosilane molecule. The γ -aminopropyltrimethoxysilane functionalized clay was prepared by refluxing 1 g of homoionic Ba clay in 25 mL of dry toluene and 1 mL of APTES under argon atmosphere, at 220°C for 12 hours. After slow cooling, the solid was recovered by filtration and washed several times with toluene to remove unreacted APTES. It was then dried overnight (12 hours) at 120°C . The collected material denoted Ba-NH, was characterized by Fourier Transform Infrared (FT-IR) on a PerkinElmer Model spectrum 100 series, Thermal gravimetric analysis (TGA) performed on a Setaram TGA92 Thermobalance, BET method on a Coulter SA 3100 and electrochemistry.

b) Preparation of nanogold particles

The glasswares used in the following procedures were cleaned in a bath of freshly prepared 3: 1 HNO_3 : HCl , rinsed thoroughly in H_2O and dried prior to use. Nanogold particles were prepared according to the literature with minor modification [35]. Briefly an acidic solution of HAuCl_4 (0.05 M) was added to basic solution of NaBH_4 (0.05 M) (1:1) under constant stirring, and a wine red solution of

nanogold was obtained and stored at 4°C. The prepared AuNPs were characterized using high resolution transmission electron microscopy (HR TEM with Technai G2 F20X-TWIN MAT 200 kV) and ultraviolet-Visible (UV-vis) spectroscopy using Nicolet Evolution 100 (Thermo Electron Cooperation).

c) Preparation of organoclay nanogold composite

The organoclay nanogold composite was prepared by suspending 20 mg of Ba-NH in a few millilitres of aqueous nanogold solution under stirring. The suspension was sonicated for 45 minutes at room temperature. Two organoclay nanogold composite samples (Ba-NH/AuNP I and Ba-NH/AuNP II) using different amount nanogold suspension have been prepared. Ba-NH/AuNP I was obtained by suspending organoclay in 3 mL of nanogold solution and then the suspension was diluted by adding 2 mL distilled water to the obtained suspension, while sample II corresponds to a situation where the same amount of organoclay was suspended in 5 mL of nanogold solution without any dilution. The suspension was allowed to rest at room temperature for few minutes and the supernatant was collected and characterized by UV –vis.

2.3. Electrode preparation

A glassy carbon electrode (GCE) was used as substrate for the sensor construction. Prior to use, the bare GCE was polished to a mirror-like surface with aqueous alumina slurry of three grain sizes (1, 0.3 and 0.05 μm) on a wet polishing cloth, followed by thorough rinsing with distilled water. After that, the electrode was sonically cleaned in 1:1 water-ethanol for 20 minutes to remove any traces of alumina. The thin organoclay nanogold composite (Ba-NH/AuNP) film working electrode was prepared by drop coating. Film deposition was performed by dropping some microliters of organoclay nanogold suspension (5 mg/ mL) onto the glassy carbon surface (\O 3 mm). The coating was allowed to dry at room temperature for 1 hour. In order to generate aldehyde terminal groups which can crosslink further with anti-CEA, 5 μL of 2.5 % glutaraldehyde was drop-coated on the organoclay nanogold film and allowed to dry at room temperature. The functionalized GCEs were then immersed in anti-CEA solution at 4 °C overnight to attach antibody. At last the immunosensors denoted GCE/Ba-NH-AuNP/Glu/anti-CEA was incubated in 10 mg/mL of BSA at room temperature to block possible remaining active sites of glutaraldehyde and avoid non specific adsorption. The resultant immunosensors were stored at 5 °C when not in use.

Organoclay free nanogold particles was not used in biosensor construction because it was found to be unstable in aqueous media ($\text{pH} < 4$) as reported in the literature [34].

2.4 Electrochemical biosensing

Electrochemical measurement was carried out in an electrochemical cell at room temperature by cyclic voltammetry (CV), square wave voltammetry (SWV) and electrochemical impedance spectroscopy (EIS). The immunosensing was perform by incubating the immunosensor in a solution

containing CEA at the room temperature for an appropriate duration and the detection of CEA level was determined by detecting the change in reduction current before and after the immunosensing in a solution containing an electrochemical sensor. The immunosensor response to CEA was calibrated using SWV responses. The nature of the bioelectrode and its charge transfer properties were modeled to appropriate electrical circuit using EIS data.

Cyclic voltammetry (CV) and all amperometric experiments were conducted using a BAS 100 potentiostat electrochemical analysis system. Measurements were performed in a conventional three electrode cell assembly consisting of Ag/AgCl reference electrode, a platinum wire counter electrode and a modified glassy carbon as working electrode.

3. RESULTS AND DISCUSSION

3.1 Organoclay nanogold composite film properties

FTIR was used to verify the grafting process and to identify the different functional groups available on materials. FTIR spectra of the pristine clay (Ba) and the organoclay were compared (figure 1B). The stretching OH vibrational mode of structural hydroxyls occurred at 3630 cm^{-1} with a component at 3697 cm^{-1} , more pronounced for Ba clay. At 1590 cm^{-1} in organoclay spectra, one can observe the deformation of NH_2 with a shoulder at 1520 cm^{-1} . Aliphatic groups ($-\text{CH}_2$) give rise to a doublet at 2938 and 2853 cm^{-1} in the same spectra corresponding to asymmetric and symmetric stretching. All these observations indicated the grafting of amino organosilane on clays.

The thermogravimetric analysis (figure 1B) of Ba and Ba-NH was run. TG curves of pristine (curve (a)) and grafted clay (curve (b)) exhibited weight losses of 17% and 21% respectively over a wide temperature range ($30 - 800\text{ }^\circ\text{C}$). The main loss of about 12 % below $250\text{ }^\circ\text{C}$ in the TG of Ba has been assigned to the removal of surface and interlayer molecular water. The TG of Ba is also marked by two peaks at 520 and $709\text{ }^\circ\text{C}$, characteristic of smectite. Above $200\text{ }^\circ\text{C}$, additional mass loss was observed at $330\text{ }^\circ\text{C}$ for the grafted clay compared to the unmodified clay. This is typical of the organoclay and indicates how much the organic agent has been loaded on clay particles.

N_2 adsorption desorption studies were carried out at 77 K on the pristine and modified clay. The inset of figure 1B shows the curves recorded. It clearly appears that the isotherm on curve (a) has a large hysteresis loop compared to that of curve (b), indicating the presence of framework mesopores with some micropores contribution. Upon modification with APTES, the surface area and the total volume of the pristine decreased from 88 to $28\text{ m}^2/\text{g}$ and from 0.15 to $0.11\text{ cm}^3/\text{g}$ respectively. The amount of grafted molecule was evaluated by elementary analysis and was found to contain 1.35 mmol/g of clay.

HR-TEM was performed to characterize the shape and size of the nanogold. The result is shown below (figure 2A). It is obvious that no particle agglomeration appeared, suggesting that the nanogold was stable in aqueous solution. The diameter of nanogold ranges from 3.6 to 4.8 nm . The nanogold nature was confirmed by EDX analysis (not shown).

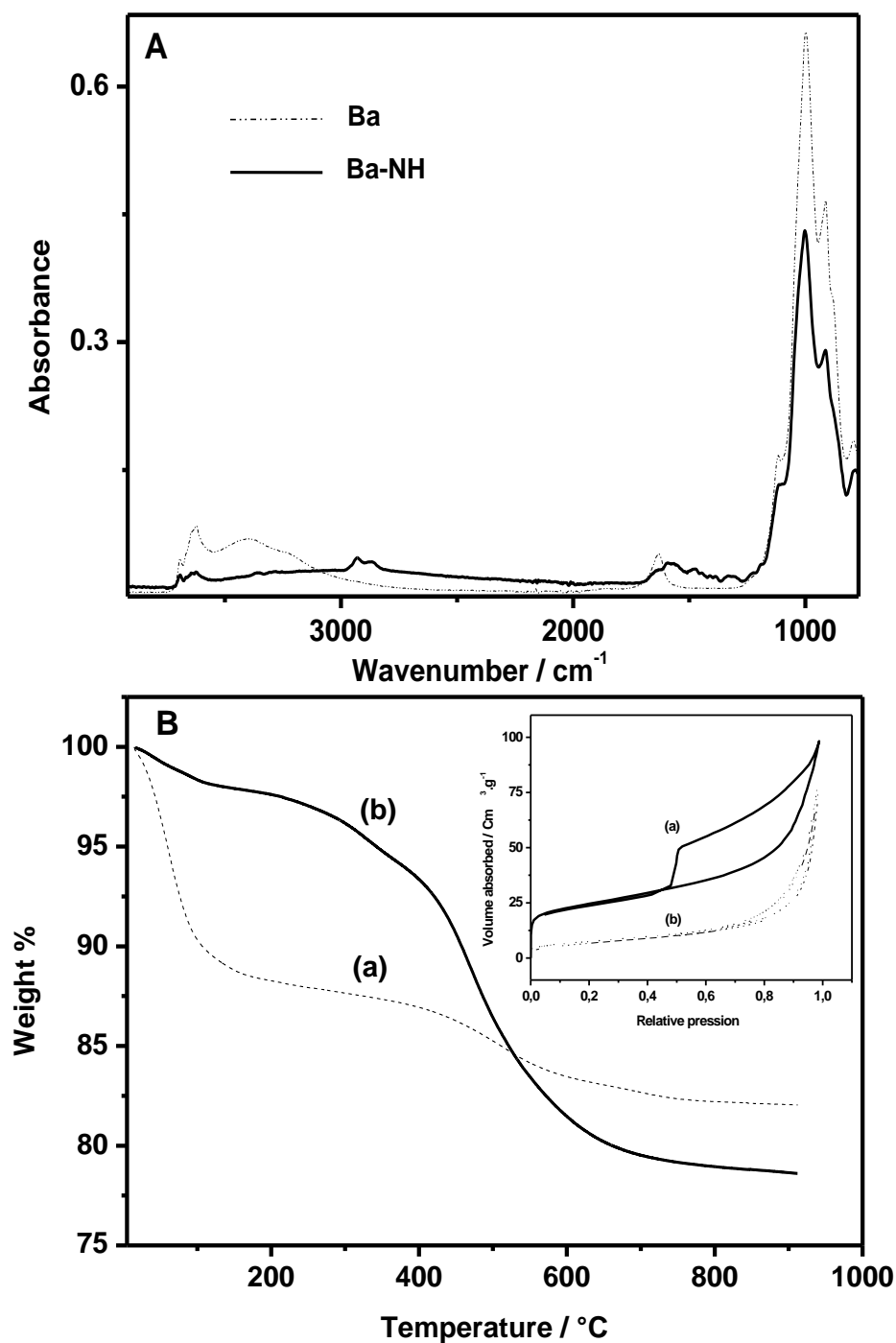


Figure 1. (A) FT-IR and (B) TGA of pristine clay (Ba) and organoclay bearing amine function (Ba-NH). Inset shows the nitrogen adsorption-desorption isotherms recorded for (a) Ba and (b) Ba-NH

The nanogold particles with size less than 5 nm were characterized by UV-vis and HR TEM. The UV-vis absorption of nanogold particles in aqueous solution exhibited a distinct surface plasmon absorption band, with the maximum absorbance at about 510 nm (curve a, figure 2B) consistent with

that reported in literature. Interestingly, the UV vis spectrum of the supernatant obtained after organoclay was suspended in nanogold solution, did not show any absorption peak (curva (b)), figure 3B). The results showed that the AuNP were adsorbed onto the Ba-NH organoclay by chemisorptions type interactions between NH₂ group and AuNP[36]

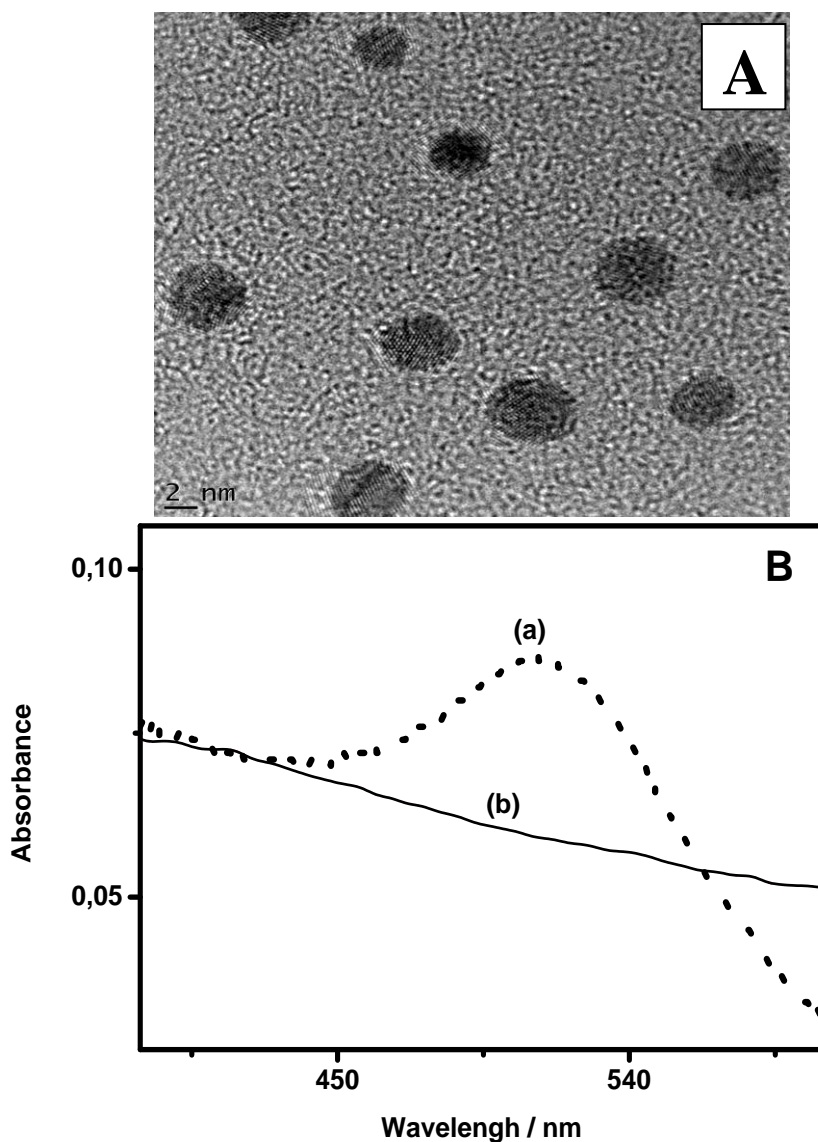


Figure 2. TEM image of nanogold particles (A) and UV-vis absorption spectra (B) of nanogold solution (a) and supernatant solution obtained after treatment of nanogold with organoclay

As prepared organoclay nanogold composite (Ba-NH-AuNP) has to be used to form film on electrode, a preliminary investigation of the permeability of Ba-NH and Ba-NH-AuNP toward an anionic probe was carried out in order to test their ability to form a stable and thin film on the GCEs surface. This was done by examining the incorporation of $[\text{Fe}(\text{CN})_6]^{3-}$ ions into the film on the electrode surface, by recording series of cyclic voltammograms in diluted solution of $[\text{Fe}(\text{CN})_6]^{3-}$.

Figure 3 below displays multi-sweep cyclic voltammograms recorded using bare and modified glassy carbon electrode. The incorporation of the negative charged probe $[\text{Fe}(\text{CN})_6]^{3-}$ into Ba-NH film was confirmed by the growth of cathodic and anodic peaks upon repetitive potential scans. The maximum steady state value was reached after *ca* 30 cycles and was about two times higher than that recorded on bare glassy carbon. These observations clearly demonstrate the stability of the film on the substrate and indicate an effective anionic preconcentration capability of the positively-charged Ba-NH organoclay.

When GCEs was coated with nanogold organoclay composite, a continuous increase in the CV peak heights was also observed on repetitive potential scanning and reached steady state values only after about 10 cycles.

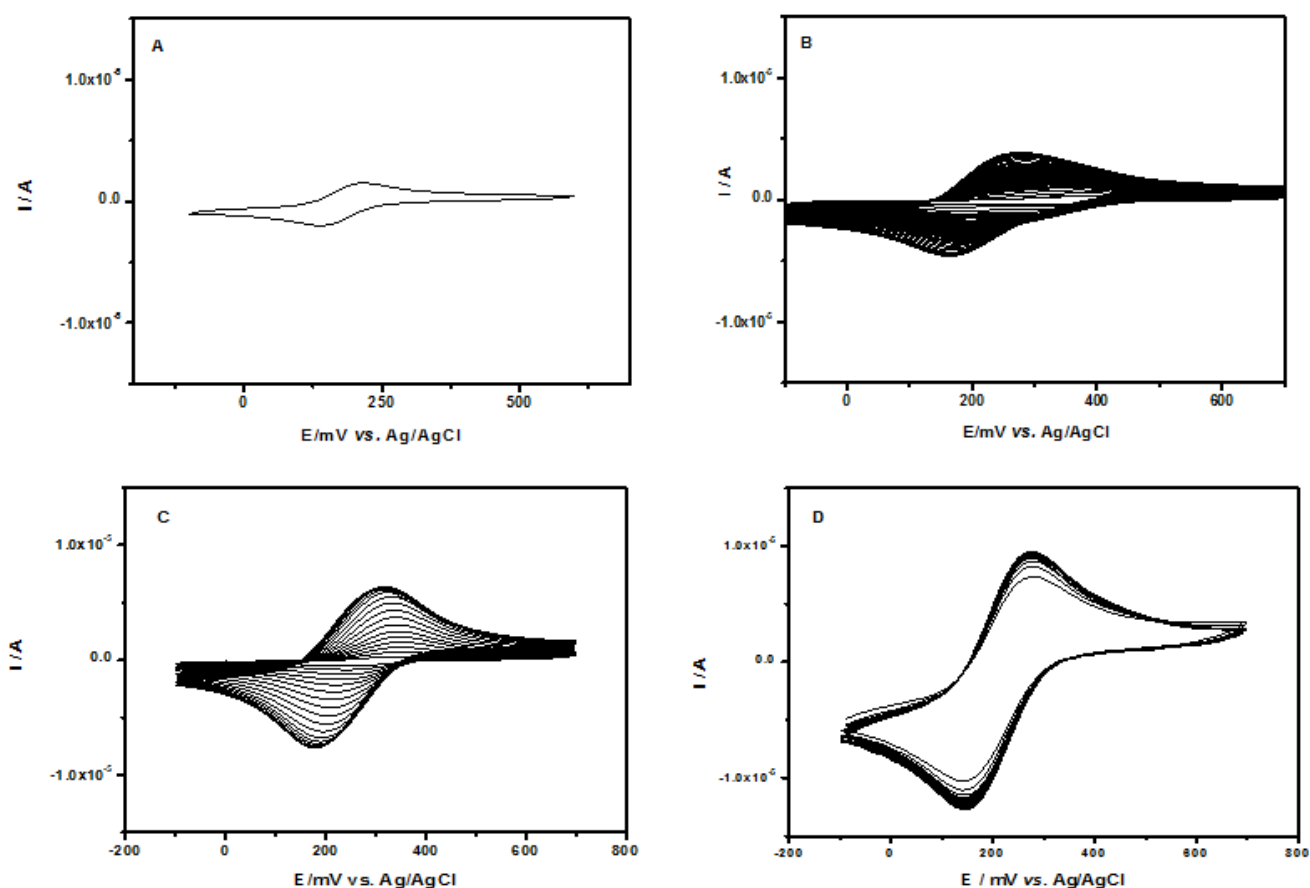


Figure 3. Multisweep cyclic voltammograms recorded in 0.1 mmol/L $\text{Fe}(\text{CN})_6^{3-}$ using A) bare GCE, B) GCE/Ba-NH, C) GCE/Ba-NH-AuNP1 and D) GCE/Ba-NH-AuNP2. The curves were obtained in 0.01 mol /L KCl used as supporting electrolyte, at a scan rate of 50 mV s^{-1} .

The peak current obtained upon saturation of the film was about five times higher than that recorded with bare GCE and peak to peak separation ($\Delta E = E_{p_a} - E_{p_c}$) was found to decrease compared to that obtained with GCE/Ba-NH and bare GCE electrodes, highlighting the beneficial role of nanogold in electron transfer. Interestingly, when the glassy carbon electrode was overcoated with Ba-

NH-NGP₂, well defined CV peak were observed not to growth upon repetitive scanning potential, although peak current was found to be more important compared to that obtained with GCE/Ba-NH-NGP₁. This behavior suggests that all amino groups available on organoclay were involved in amino nanogold interactions.

Strikingly well defined CV peaks were recorded with GCE/Ba-NH-NGP₁ over-coated with glutaraldehyde negatively charged (supplementary figure, Fig. S1), but these peaks were observed not to grow on repetitive potential scanning, likely because on one hand free amino groups on Ba-NH have interacted with aldehyde groups of glutaraldehyde and on the other hand nanogold in the nanocomposite acts as a conductive wire or electron-conducting tunnel, which makes it easier for the electron transfer to take place.

3.2 Electrochemical responses of CEA immunosensor

Electrochemical impedance spectroscopy is an effective method to probe and model the interfacial properties of the surface modified electrode. Figure 4 shows the result of Faradic impedance spectroscopy on a bare glassy carbon electrode (GCE), GCE/Ba-NH-AuNP, GCE/Ba-NH-AuNP/Glu and GCE/Ba-NH-AuNP/antiCEA in the presence of 5 mM Fe(CN)₆^{4-/3-} (1:1) as a redox probe in 0.01 M phosphate buffer containing 0.1 M KCl.

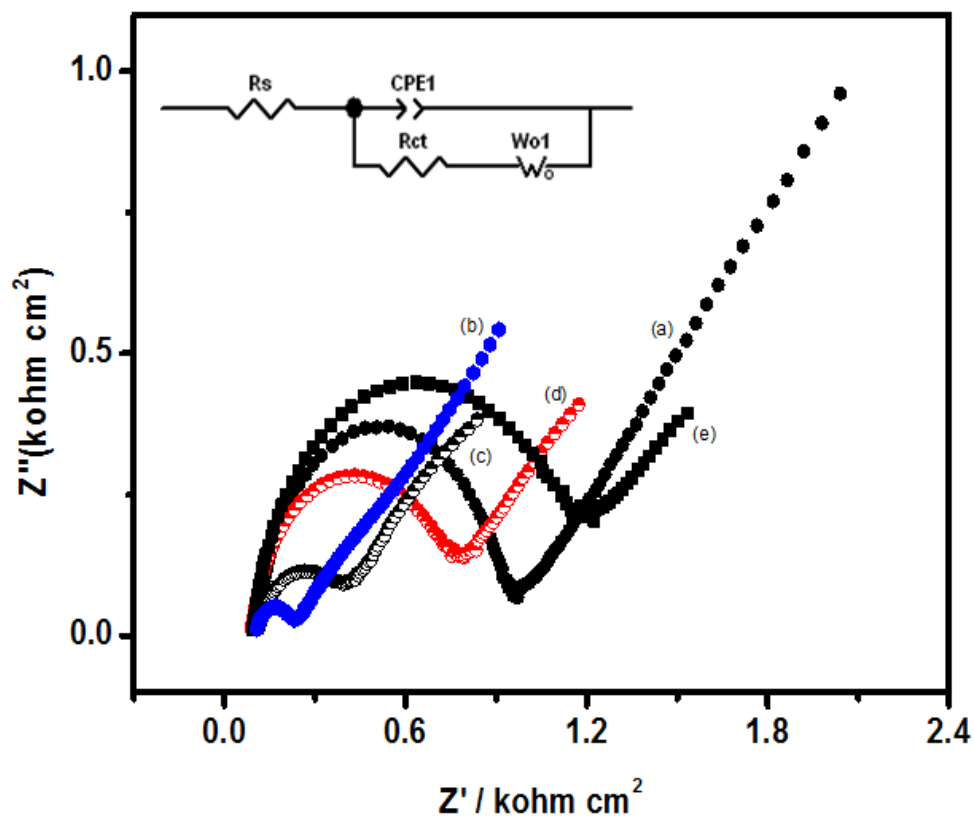


Figure 4. ESI of different electrodes: (a) Bare GCE, (b) GCE/ Ba-NH AuNP, (c) GCE/Ba-NH AuNP/Glu, (d) GCE/ Ba-NH AuNP /Glu/AntiCEA, (e) GCE/ Ba-NH AuNP /Glu/AntiCEA-CEA in 5 mM Fe(CN)₆^{4-/3-} (PBS pH 6.5)

From the figure above one can observe that the bare GCE exhibited a large semicircle at high frequencies, indicating a high resistance on bare GCE. After the modification of the GCE with a film of organoclay nanogold composite, a remarkable decrease of the semicircle diameter was observed, this proved that the composite was beneficial to the electron transfer. After the incubation of organoclay nanogold film electrode in CEA antigen solution, the diameter of the semicircle remained unchanged, suggesting that no CEA antigen were immobilized on organoclay nanogold modified GCE via AuNP as reported in elsewhere [20; 22; 23; 27; 37; 38; 39; 40; 41; 42]. Interestingly, when a layer of glutaraldehyde was coated on organoclay nanogold composite modified electrode, the resistance increased slightly owing to the increase of the film thickness which hindered the electron transfer as observed on CV. After the immobilization of Anti CEA as a biomacromolecule with weak electroactivity via the coupling agent glutaraldehyde on the composite modified electrode, the EIS presented an increase in resistance. Glutaraldehyde is bifunctional molecule and its aldehyde groups interacted with free amino groups available on Ba-NH-AuNP and amino group of anti CEA, which linked anti CEA to film modified electrode. A further increase was noticed when the immunosensor was incubated in CEA antigen. On the basis of these results, it could be clearly confirmed that immune-complexation reaction between CEA antigen and CEA antibody took place. The typical electrochemical interface can be represented as an electrical circuit as shown in the inset of figure 4.

The figure 5 shows the cyclic voltammograms (CVs) of different electrodes in different conditions in $[\text{Fe}(\text{CN})_6]^{3-/4-}$. Here, CV was used to investigate the electrochemical behaviours of $[\text{Fe}(\text{CN})_6]^{3-/4-}$ after each assembled step. The redox-label $[\text{Fe}(\text{CN})_6]^{3-/4-}$ revealed a reversible CV at the bare GCE (curve a). A couple of well-defined redox peaks was observed at the bare electrode with distinct cathodic peak (i_{pc}) and anodic peak current (i_{pa}) values and a peak to peak separation ΔE_p of 157 mV.

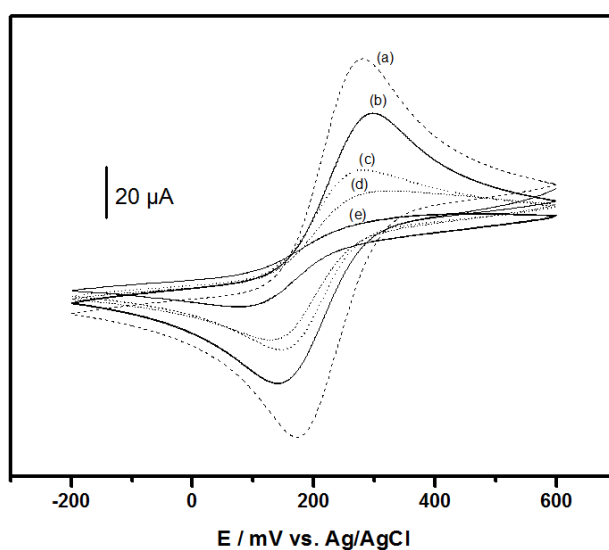


Figure 5. Cyclic voltammograms of (a) GCE/ Ba-NH nanoAu, (b) Bare GCE, (c) GCE/Ba-NH AuNP/Glu, (d) GCE/ Ba-NH AuNP /Glu/AntiCEA, (e) GCE/ Ba-NH AuNP /Glu/AntiCEA incubated in 2 ng/ L of CEA in $\text{Fe}(\text{CN})_6^{4-/3-}$ (pH 6.5). Scan rate $50 \text{ mV} \cdot \text{S}^{-1}$

After the pretreated GCE was modified with organoclay nanocomposite, the peak current increased greatly and the peak to peak separation was reduced by 52 mV compared to CV recorded with bare GCE. These results indicate that the introduction of the nanogold in the organoclay played a role in the increase of the electroactive surface area and provided the conducting bridges for the electron-transfer of $[\text{Fe}(\text{CN})_6]^{3-/4-}$.

Contrarily, although a well definite CV (curve c) was observed when the organoclay nanogold composite modified electrode was treated with glutaraldehyde, the peak current decreased by 56 % and peak to peak separation increased ($\Delta E=135$ mV) indicating that there were lower electron transfer compared to that recorded with organoclay nanogold modified CGE. This is likely due to electrostatic repulsion between negatively charged glutaraldehyde and redox probe and to the low conductivity of glutaraldehyde film. Subsequently, when the anti-CEA was loaded and the immusensor blocked with BSA solution, a further decrease in the peak current due to the insulating protein retards the electron transfer (curve d). After the immunosensor was incubated with 20 ng.mL^{-1} CEA solution, the reduction and oxidation peak current exhibited a great decrease. This may originate from the anti-CEA and CEA reacting to produce an immunocomplex, which inhibited the electron-transfer. One should note that with the antibody and the antigen-antibody modified electrodes, the cyclic voltammograms remained constant upon cycling a decrease in current peak was observed while the peak to peak potential separation remained nearly unchanged.

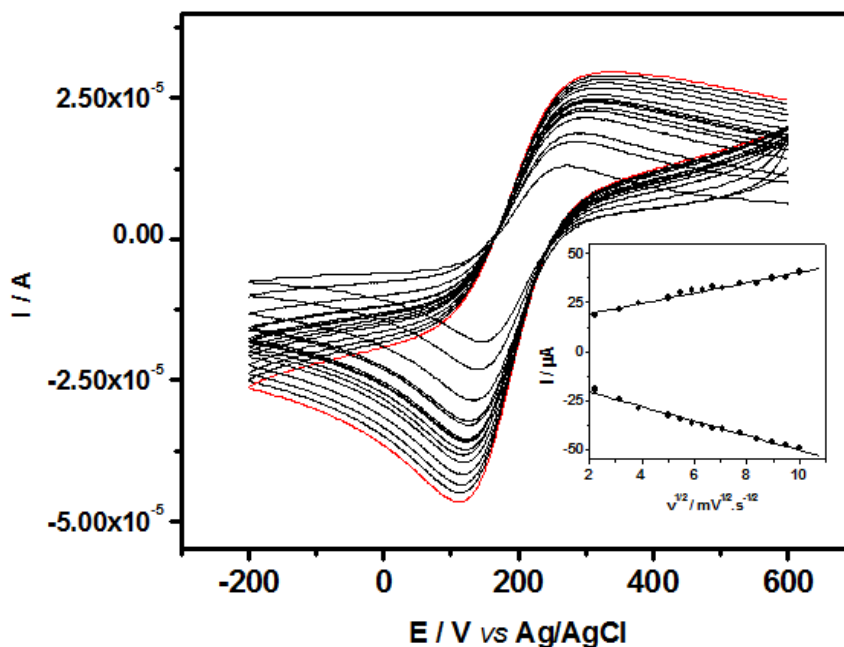


Figure 6. Cyclic voltammograms of GCE/ Ba-NH AuNP /Glu/AntiCEA at different scan rates in $\text{Fe}(\text{CN})_6^{4-/3-}$ (pH 6.5). The inset shows the dependence of redox peak currents on the square root of the scan rate

Figure 6 depicts the CVs of the prepared immunosensor in $5 \text{ mM } [\text{Fe}(\text{CN})_6]^{3-/4-}$ solution (pH 7.0) at different scan rates. It is evident that ferricyanide ions presented a well-defined reversible redox

wave in this study. Furthermore, both the anodic and cathodic peak currents were directly proportional to the scan rates in the range of 5 to 100 mV s^{-1} , as shown in the inset of figure 6, suggesting a surface-confined electrochemical process.

To acquire an optimal analytical performance of the as-prepared immunosensor, some important parameters including the incubation times and incubation temperature for antigen-antibody reaction and pH of the assay solution were studied. It was found that the maximum response occurred after 20 minutes of incubation of the immunosensors in antigen solution at 35 °C at pH 6.5.

After optimization of the experimental parameters, the immunosensor was used to detect CEA. Square wave technique was employed to investigate the response of immunosensor to CEA. Figure 7 shows the square wave voltammograms after the immunosensor was incubated in different CEA solutions.

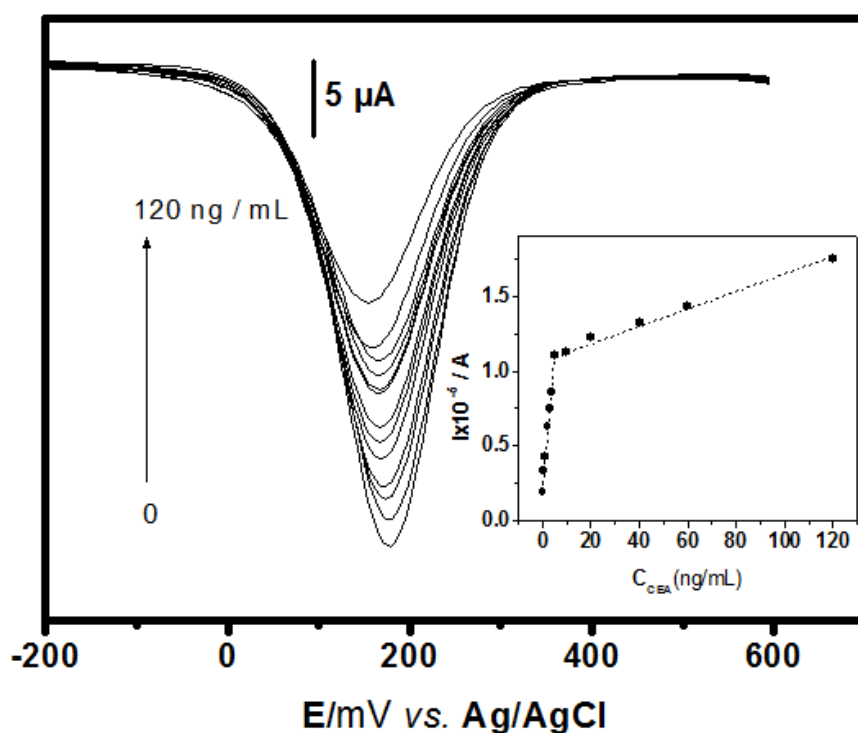


Figure 7. SQW voltammograms of the immunosensor GCE/ Ba-NH AuNP /Glu/AntiCEA in 0.01 M KCl (0.01M PBS) after incubation in different concentrations of CEA. Inset shows calibration curves.

The blank response was obtained when the immunosensor was incubated without any CEA in the incubation solution. Then, with the increase of CEA concentration, the current response decreased significantly due to the formation of the anti-CEA and CEA immunocomplex on the electrode surface, which forms a barrier for the electrons. The calibration plots were obtained by recording the change of current response (ΔI) vs. the different concentrations of CEA standard solutions. As shown in the inset, under optimal conditions, the linear range spans the concentration of CEA from 0.05 to 5.0 ng / mL and 5.0 to 120 ng / mL with correlation coefficients 0.991 and 0.998 respectively. The linear slopes

were found to be $1.579 \mu\text{A} (\text{ng/mL})^{-1}$ and $0.056 \mu\text{A} (\text{ng/mL})^{-1}$ respectively. A low detection limit of 0.02ng/mL was determined at a signal/noise ratio of 3.

Moreover, the performances of the developed CEA immunosensors were also compared with those of other immunosensors for the detection of CEA with various antiCEA modified electrodes, as shown in Table 1 summarizing the linear range, the detection limits and sensitivity. The comparative data suggested that the current method obviously exhibited a high sensitivity, a wider linear range and lower detection compared to some immunosensors prepared by immobilizing anti CEA using glutaraldehyde as cross linking agent [43; 44; 45]

or nanogold particles and doped with redox mediator [27; 38; 39; 40; 46; 47; 48; 49]. This can be attributed to a stable Ba-NH-AuNP/Glu film which increased the immobilized amount of antibody via the cross linking agent, retained its activity and enhanced current response.

The reproducibility of the developed immunosensors was investigated, by evaluating the sensitivity of five antiCEA organoclay nanogold composite films modified electrodes prepared independently. On recording the corresponding amperometric response in 0.01 mol L^{-1} phosphate buffer pH 6.5 after incubating the immunosensors in 5 ng/mL of CEA for 20 minutes at 35°C , it was observed that the relative standard deviation of the sensitivity of the affinity biosensor was 5.4 %.

To examine the selectivity of the immunosensors, the sensor was incubated with 2 ng/mL CEA solution in the presence of some interferences potentially coexisting with CEA such as ascorbic acid ($20 \mu\text{g/mL}$). The current ΔI obtained with interfering agent were found to increase only by 0.3 % of ΔI obtained without interfering agent.

Table 1. Comparison of analytical performances of different immunosensors for the detection of CEA. *Poly-sulfanilic acid (PSAA), toluidine blue (TB), multi-walled carbon nanotubes (MWNTs), chitosan (CHIT), 3- mercaptopropanesulfonic, sodium salt (MPS), prussian blue (PB), thionine (Thi), poly(toluidine blue O (PTOB), poly(diallyldimethylammonium chloride) (PDDA)

Immunosensors fabrication*	Linearity range (ng mL^{-1})	Detection limit (ng mL^{-1})	Sensitivity (nA/ ng mL^{-1})	Reference
anti-CEA/AuNP TB/PSAA/GCE	0.5–5.0 ; 5.0–120.0	0.2	-	[46]
anti-CEA /AuNP /nano-CaCO ₃ /PB /GCE	0.3–20.0 ; 20.0–100.0	0.1	1870 and 35	[47]
anti-CEA/(AuNP–MWNTs–THI–CHIT) ₈ /MPS}-Au	0.5–3.0 ; 3.0–120.0	0.4	-	[48]
anti-CEA/Au-NP/Thi/Chit/GCE	0.20–10.0 ; 10.0–160.0	0.08		[49]
HRP- anti CEA/Glu/ Thi / GCE	0.5 to 3.0 ;3.0 to 167	0.1	130 and 54.9	[45]
anti-CEA/AuNP/PB/NG/GCE	0.5–10 and 10–120	0.2	832	[39]
anti-CEA/AuNP/PB/CS-MWNT-AuNP/GCE	0.3 to 120	0.1	688.6	[40]
anti-CEA/AuNP/Chit/NG/GCE	0.2–120.0	0.06	1310.0	[27]
anti-CEA/Glu/ meso-Al ₂ O ₃ / GCE	0.04 to 10	0.03	-	[44]
anti-CEA/AuNP/PTOB/DNA–PDDA/GCE	0.5–120	0.3	106	[38]
HRP-anti-CEA/sol–gel/GE	0.5 to 3.0 and 3.0 to 120	0.4	1120 and 88	[48]
anti-CEA/AuNP/PTC–NH ₂ /PB/GCE	0.05–2.0 and 2.0–40	0.018	-	[42]
anti-CEA/Glu/GPMS/Fe ₃ O ₄ –SiO ₂ /CPE	1.5–60	0.5	-	[43]
anti-CEA/Glu/AuNP/AuNP–HN–Ba/GCE	0.05– 5.0;5.0–120.0	0.02	1579 and 56	This work

4. CONCLUSION

Colloidal gold nanoparticles were demonstrated to be stable in amino grafted clay matrix with an orderly structural organization. This nanocomposite was used to elaborate an affinity and catalytic biosensors. Due to its good biocompatibility and catalytic properties, organoclay nanogold composite showed good catalytic property towards $\text{Fe}(\text{CN})_6^{4-/3-}$, so a simple label free electrochemical immunosensor for rapid detection of cancer tumor was constructed by immobilizing anti CEA on the organoclay nanogold electrode modified GCE via glutaraldehyde. The immunosensor showed good precision and acceptable sensitivity, which were due to the advantages of colloidal gold nanoparticles organoclay matrix and the stability of organoclay nanogold composite and glutaraldehyde films.

ACKNOWLEDGEMENTS

The authors would like to acknowledge the financial support of the Organisation for the Prohibition of Chemical Weapons (OPCW), through project L/ICA/ICB/168938/11

References

1. P.K. Ghosh, A.J. Bard, *J. Phys. Chem* 88 (1984) 5519
2. Z. Navratilova, P. Kula, *Electroanalysis* 15 (2003) 837
3. J.-M. Zen, A.S. Kumar, *Anal. Chem.* 76 (2004) 205A
4. C. Mousty, *Apply Clay Science* 227 (2004) 159
5. E. Ngameni, I. K. Tonlé, J. T. Apohkeng, G. B. Bouwé, A. T. Jieumboue, A. Walcarius, *Electroanalysis* 18 (2006) 2243
6. H. L. Tcheumi, I. K. Tonle, E. Ngameni, A. Walcarius, *Talanta* 81 (2010) 972
7. M. G. d. Fonseca, J. S. Barone, C. Airoidi, *Clays Clay Miner* 48 (2000) 638.
8. S. L. Burkett, A. Press, S. Mann, *Chem. Mater.* 9 (1997) 1071.
9. K. A. Carrado, L. Xu, R. Csencsits, J. V. Muntean, *Chem. Mater.* 13 (2001) 3766.
10. S. K. Lee, S. J. Kim, *Appl. Clay Sci.* 22 (2002) 55.
11. J. Kemmegne-Mbouguen, E. Ngameni, A. Walcarius, *Biosens. Bioelectron.* 23 (2007) 269
12. J. Kemmegne-Mbouguen, E. Ngameni, A. Walcarius, *Anal. Chim. Acta* 578 (2006) 145
13. J. Kemmegne-Mbouguen, I.T. Kenfack, A. Walcarius, E. Ngameni, *Talanta* 85 (2011) 754
14. S.Q. Hu, J.W. Xie, Q.H. Xu, K.T. Rong, G.L. Shen, R.Q. Yu, *Talanta* 61 (2003) 769
15. J. J. Storhoff, R. Elghanian, R.C. Mucic, C. A. Mirkin, R. L. Letsinger, *J. Am. Chem. Soc.* 120 (1998) 1959
16. X. Gao, Y. Zhang, H. Chen, Z. Chen, X. Lin, *Anal. Biochem.* 414 (2011) 70
17. G. K. Ahirwal, C. K. Mitra, *Sensors* 9 (2009) 881
18. Y. Zhuo, R. Yuan, Y.Q. Chai, A.L. Sun, Y. Zhang, J.Z. Yang, *Biomaterials* 27 (2006) 5420
19. S. Zhao, K. Zhang, Y. Bai, W. Yang, C. Sun, *Bioelectrochem.* 69 (2006) 158
20. M. C. Daniel, D. Astruc, *Chem. Rev.* 104 (2004) 293
21. S. Xu, X. Han, *Biosens. Bioelectron.* 19 (2004) 1117
22. R. Y. Xiulan He, Y. Chai, Y. Shi, *J. Biochem. Biophys. Methods* 70 (2008) 823
23. Y. Liu, R. Yuan, Y. Chai, C. Hong, K. Liu, S. Guan, *Microchim Acta* 167 (2009) 217
24. P. Lv, L. Min, R. Yuan, Y. Chai, S. Chen, *Microchim Acta* 171 (2010) 297
25. Q. Cao, H. Zhao, Y. Yang, Y. Hea, N. Dinga, J. Wanga, Z. Wu, K. Xiang, G. Wange, *Biosens. Bioelectron.* 26 (2011) 3469
26. Y.R. Yuan, R. Yuan, Y.Q. Chai, Y. Zhuo, X.M. Miao, *J. Electroanal. Chem.* 626 (2009) 6

27. X. He, R. Yuan, Y. Chai, Y. Shi, *J. Biochem. Biophys. Methods* 70 (2008) 823
28. N. Gan, J. Hou, F. Hu, L. Zheng, M. Ni, Y. Cao, *Molecules* 15 (2010) 5053
29. V. Moro, J. P Vuillez, C. A. Delord, C. Brambilla, *Lung Cancer* 13 (1995) 169
30. B.Nisman, J.Lafair, T.Peretz, I.Roisman, V. Barak, *Eur. J. Cancer* 31 (1995) s263
31. E. Eppler, H. Hörig, H.L. Kaufman, P. Groscurth, L. Filgueira, *Eur. J. Cancer* 38 (2002) 184
32. K. Bremer, S. Nicus, G. Bremer, *Eur. J. Cancer* 31 (1995) s262
33. C. Carneiro, L. Costa, M. Melo, A. Quintela, I. Miranda, M. Jorge, *Eur. J. Cancer A* 34 (1998) s43
34. I. K. Tonle, E. Ngameni, D. Njopwouo, C. Carteret, A. Walcarius, *Phys. Chem. Chem. Phys.* 5 (2003) 4951
35. M. N. Martin, J. I. Basham, P. Chando, S. K. Eah, *Langmuir* 26 (2010) 7410
36. J. Wang, *Electroanalysis* 17 (2005) 7-14.
37. Y. Li, W. K. Yang, M. Q. Fan, A. Liu, *Anal. Sci.* 27 (2011) 1223
38. N. Li, H. Zhao, R. Yuan, Z. Peng, Y. Chai, *Electrochim. Acta* 54 (2008) 235
39. P. Lv, L. Min, R. Yuan, Y. Chai, S. Chen, *Microchim Acta* 171 (2010) 297
40. Z. Song, R. Yuan, Y. Chai, B. Yin, P. Fu, J. Wang, *Electrochim. Acta* 55 (2010) 1778
41. X. Che, R. Yuan, Y. Chai, J. Li, Z. Song, J. Wang, *J. Colloid Interface Sci.* 345 (2010) 174
42. Z. Liu, R. Yuan, Y. Chai, Y. Zhuo, C. Hong, X. Yang, *Sensors Actuators B* 134 (2008) 625
43. J. Pan, Q. Yang, *Anal. Bioanal. Chem.* 388 (2007) 279
44. Y. Dai, H. Li, D. Wu, R. Li, Y. Zhao, B. Liu, Y. Cai, M. Yang, B. Du, Q. Wei, *Electroanalysis* 23 (2011) 1602
45. F.Y. Zong Dai, Hua Yu, Xiaoya Hu, Huangxian Ju, *J. Immunol. Methods* 287 (2004) 13
46. X.L. Li, R.Yuan, Y.Q. Chai, L.Y. Zhang, Y. Zhuo, Y. Zhang, *J. Biotechnol.* 123 (2006) 356
47. G. Zhang, R. Yuan, Y. Chai, K. Liu, S. Ling, *Microchim. Acta* 165 (2009) 53
48. F. Tan, F. Yan, H. Ju, *Electrochem. Commun.* 8 (2006) 1835
49. Y. Liu, R. Yuan, Y. Chai, C. Hong, K. Liu, S. Guan, *Microchim. Acta* 167 (2009) 217